JOURNAL OF SOLID STATE CHEMISTRY 67, 42–50 (1987)

Structural and Dynamical Studies of δ-Bi_2O_3 Oxide-Ion Conductors

II. A Structural Comparison of $(Bi_2O_3)_{1-x}(M_2O_3)_x$ for M = Y, Er, and Yb

P. D. BATTLE,*,† C. R. A. CATLOW‡ AND L. M. MORONEY§

† *Department of Inorganic and Structural Chemistry, Leeds University, Leeds LS2 9JT, United Kingdom;* ‡ *Department of Chemistry, Keele University, Keele, Staffordshire ST5 5BG, United Kingdom; and* § *N.S.L.S., Brookhaven National Laboratory, Upton, New York 11973*

Received February 7, 1986; in revised form June 18, 1986

We report the results of diffuse elastic neutron scattering studies of the superionic solid solutions $(Bi_2O_3)_{1-x}(Er_2O_3)_x$ and $(Bi_2O_3)_{1-x}(Yb_2O_3)_x$, and also the result of a Bragg diffraction study of $(Bi_2O_3)_{0.75}(Er_2O_3)_{0.25}$. All the data suggest that Er^{3+}-doped δ-Bi_2O_3 is structurally very similar to the fluorite-related solid solution $(Bi_2O_3)_{1-x}(Y_2O_3)_x$ studied previously, both in terms of the average structure as determined by Bragg scattering and in terms of local ordering on the anion sublattice as detected by diffuse scattering. The ordered regions are described as microdomains of a rhombohedral phase. The Yb^{3+}-doped materials also show short-range anion ordering, but over shorter distances than in the other two cases. There is evidence of cation ordering between Bi^{3+} and Yb^{3+} near the low-dopant boundary of the fluorite phase. The possible use of quasi elastic neutron scattering to monitor oxide-ion transport in the system $(Bi_2O_3)_{1-x}(Er_2O_3)_x$ is discussed. © 1987 Academic Press, Inc.

Introduction

The high temperature δ-phase of Bi_2O_3 (stable above 1003 K) is the best oxide-ion conductor known (*1*) with a conductivity of $\sim 1\ \Omega^{-1}\ cm^{-1}$ at 1023 K compared to a value of $10^{-4}\ \Omega^{-1}\ cm^{-1}$ for the widely used CaO/ZrO_2 system (*2*). A number of cation dopants, specifically Y^{3+} and the trivalent ions of smaller rare earths, lower the temperature of transition from the poorly conducting low-temperature phase to the super ionic δ phase (*1*) and Y_2O_3-doped Bi_2O_3, for example, is stable with the face-centered-cubic, fluorite-like structure of the δ-phase at room temperature for dopant levels of between 25 and 42 mol%. However, the presence of the dopant ions raises the Arrhenius energy for oxygen migration and hence lowers the ionic conductivity and our aim is to elucidate the structural changes which accompany this drop in conductivity. Previous structural studies (*3, 4*) on both δ-Bi_2O_3 itself and on its solid solutions with Y_2O_3 have revealed significant anion relaxation along the ⟨111⟩ directions of the cubic unit cell, the number of relaxed anions decreasing with decreasing conductivity and increasing dopant concentration. The doped materials, but not δ-Bi_2O_3 itself, also appear to contain a small number of anions which are slightly displaced from the octahedrally coordinated interstitial site in the fluorite structure, and there is also some evidence to suggest that the cations undergo displacements along ⟨100⟩ from their ideal positions. Careful studies using diffuse scattering techniques have shown that

* To whom correspondence should be addressed.

0022-4596/87 $3.00

Copyright © 1987 by Academic Press, Inc.
All rights of reproduction in any form reserved.

in the doped materials these displacements are not random throughout the structure, but that there are small, ordered microdomains within the overall fluorite structure of the solid solutions. Data which would permit a full determination of the microdomain structure are not yet available, but the factors which might influence it have been discussed previously (*4*). The experimental evidence presently available suggests that the structure in the microdomains of $(Bi_2O_3)_{1-x}(Y_2O_3)_x$ may be related to the rhombohedral structure of the solid solutions formed between Bi_2O_3 and larger dopant cations, both isovalent and aliovalent, e.g., Sm^{3+} and Sr^{2+} (*5, 6*). Unfortunately, although the cation framework in the aliovalent materials is well defined (*6*), X-ray diffraction has failed to produce a satisfactory description of the anion sublattice in either type of system.

The neutron scattering lengths of Bi and Y are very similar, and it is therefore likely that the ordering detected in the neutron diffuse scattering experiments performed to date occurs amongst the vacancies and oxide ions, both relaxed and unrelaxed, which make up the anion sublattice. It is also possible that the ⟨100⟩ cation displacements are ordered over short distances and contribute to the observed scattering, but our results are insensitive to cation ordering between Bi^{3+} and Y^{3+}. To probe possible ordering in the cation sublattice we have now undertaken a study of the solid solutions $(Bi_2O_3)_{1-x}(Yb_2O_3)_x$, this system being chosen because Bi and Yb have substantially neutron scattering lengths, thus increasing the sensitivity of our experiments to cation ordering. In addition, we have studied $(Bi_2O_3)_{1-x}(Er_2O_3)_x$ in greater detail than was possible in a previous structural study (*7*).

Experimental

Polycrystalline samples of $(Bi_2O_3)_{1-x}(Er_2O_3)_x$ (x = 0.4, 0.32, 0.25) and $(Bi_2O_3)_{1-x}(Yb_2O_3)_x$ (x = 0.35, 0.30, 0.25, 0.2) were prepared by firing the appropriate amounts of high purity Bi_2O_3 and M_2O_3 (M = Er or Yb) in a platinum crucible at a sintering temperature which was a function of composition (*5*). Each sample was heated at a rate of 1 K min^{-1} to a prefiring temperature of 1053 K where it was left for 16 hr before heating to the sintering temperature. After equilibration for a further 16 hr it was cooled to 773 K, at which temperature it was annealed for 24 hr. This cycle was repeated until the X-ray powder diffraction pattern of each sample contained only sharp lines characteristic of a well-crystallized face-centered-cubic structure. The unit cell parameters deduced from the powder patterns of the products are tabulated in Table I. It should be noted that the stability range of the fluorite-related phase in the Yb^{3+}-doped samples prepared in this work is much greater than that reported previously (*5*), where the solubility range for Yb_2O_3 in Bi_2O_3 was found to be anomalously small. This difference presumably stems from variations in the heat treatment of the two batches of samples. Neutron powder diffraction data were collected on the sample of $(Bi_2O_3)_{0.75}(Er_2O_3)_{0.25}$ at room temperature using the constant wavelength diffractometer (λ = 1.388 Å) D1a at ILL Grenoble. The diffuse scattering from all the samples were recorded on the diffractometer D7, also at ILL. These experiments were performed using a mean neutron wavelength of 4.85 Å, a cold Be filter being employed to minimise contamination by shorter wavelengths. The scattered neu-

TABLE I

UNIT-CELL PARAMETER (IN Å) FOR SOLID SOLUTIONS $(Bi_2O_3)_{1-x}(M_2O_3)_x$

M	0.2	0.25	0.30	0.32	0.35	0.40
Yb	5.477(4)	5.462(1)	5.437(2)	—	5.419(1)	—
Er	—	5.479(1)	—	5.451(1)	—	5.425(1)

trons were subjected to time-of-flight analysis to distinguish between elastic and inelastic scattering. Data were also collected on an empty sample can, cadmium foil and a vanadium rod to allow the differential scattering cross section of the sample relative to that of vanadium to be determined.

Results

(i) *Bragg Scattering from* $(Bi_2O_3)_{0.75}(Er_2O_3)_{0.25}$

The neutron powder diffraction profile of this sample was very similar to those recorded previously (*3, 4*) on $(Bi_2O_3)_{1-x}(Y_2O_3)_x$ with all the observed reflections being indexed in space group $Fm3m$. We refined the structure using the intensities of 20 peaks (23 reflections) and the final observed and calculated intensities are presented in Table II. The refined structural parameters which gave rise to a final R_I factor of 1.6% are listed in Table III. The model used is the same defect-fluorite as was found in the case of the Y^{3+}-doped materials (*3, 4*) and it thus includes (i) a number of anions which relax away from the regular, tetrahedral (8*c*) anion sites of the fluorite structure along ⟨111⟩ directions to occupy 32*f* sites; (ii) a number of anions displaced somewhat from the octahedral, interstitial 4*b* sites to 48*i* sites; and (iii) anions on the regular, (8*c*) fluorite site. The cations, assumed to be disordered, are again displaced along ⟨100⟩ directions from the 4*a* site to occupy 24*e* sites. The intensities presented in Table II have been corrected for absorption using the calculations of Rouse *et al.* (*8*) but the structural parameters in Table III showed no significant variation when this correction was omitted. Our model differs from that deduced in an earlier study (*7*) which used a very limited data set.

TABLE II

OBSERVED AND CALCULATED NEUTRON POWDER DIFFRACTION INTENSITIES FOR $(Bi_2O_3)_{0.75}(Er_2O_3)_{0.25}$ AT ROOM TEMPERATURE

{*h*	*k*	*l*}	I_{obs}	σI_{obs}	I_{calc}
1	1	1	10,400	129	10,400
2	0	0	177	76	193
2	2	0	13,700	148	13,700
3	1	1	6,730	119	6,660
2	2	2	255	70	282
4	0	0	1,840	87	1,780
3	3	1	1,870	84	1,910
4	2	0	611	62	616
4	2	2	2,780	91	2,900
5	1	1	1,420	80	1,500
3	3	3			
4	4	0	652	66	678
5	3	1	1,350	77	1,270
6	0	0	292	54	286
4	4	2			
6	2	0	746	60	665
5	3	3	243	56	225
6	2	2	164	52	166
4	4	4	93	54	112
5	5	1	412	67	421
7	1	1			
6	4	0	72	52	88
6	4	2	528	77	503

TABLE III

STRUCTURAL PARAMETERS FOR $(Bi_2O_3)_{0.75}(Er_2O_3)_{0.25}$ AT ROOM TEMPERATURE

	Site	*X*	*Y*	*Z*	*B* (Å²)	Occupation number
Cation	24*e*	0.045(3)	0	0	1.9(3)	2
O1	8*c*	¼	¼	¼	5.9(2)	1.97(10)
O2	32*f*	0.319(2)	0.319(2)	0.319(2)	5.9(2)	0.88(10)
O3	48*i*	½	0.32(2)	0.32(2)	5.9(2)	0.15(10)

(ii) *Diffuse Scattering from* $(Bi_2O_3)_{1-x}(Er_2O_3)_x$

The elastic component of the scattered intensity recorded in the D7 experiments is plotted as a function of Q ($= 4\pi \sin\theta/\lambda$) and 2θ in Fig. 1 for the bismuth–erbium oxide solid solutions with $x = 0.25$ and $x = 0.40$. The scattering has been scaled to the differential cross section of vanadium. The raw

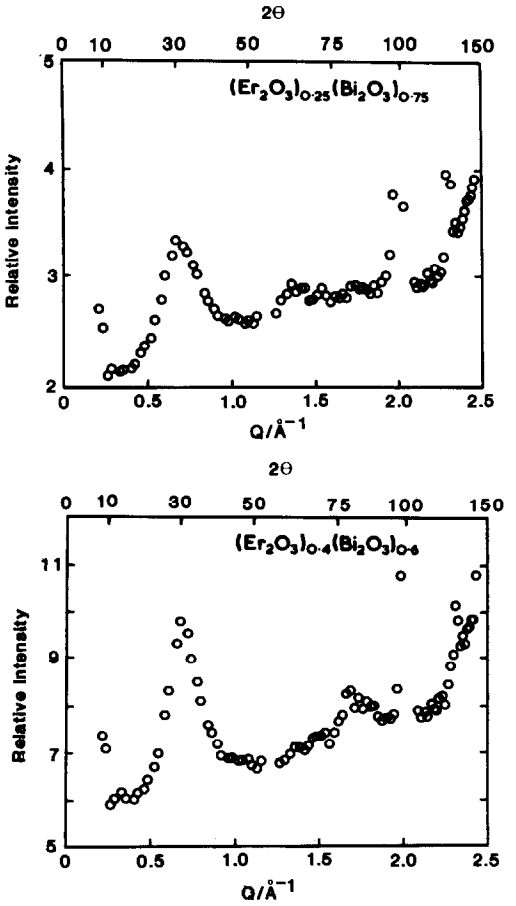

FIG. 1. Diffuse elastic scattering for $(Bi_2O_3)_{1-x}(Er_2O_3)_x$, $x = 0.25$ and 0.4, at room temperature.

data were corrected for absorption but multiple scattering corrections were not applied. The most striking feature in both patterns is the rather sharp peak at $Q \sim 0.7$ Å^{-1}. There are other clear, but less prominent, features at $Q \sim 1.4$ Å^{-1} and $Q \sim 1.7$ Å^{-1}. The (111) and (200) Bragg peaks can be seen at $Q \sim 2.0$ Å^{-1} and $Q \sim 2.3$ Å^{-1}, respectively. The presence of these peaks is due to the enforced use of a wavelength shorter than the Bragg cutoff ($=2d_{(111)}$) for the fluorite structure, and the observed scattering thus contains a component of double Bragg scattering. Fortunately, this additional scattering varies smoothly with Q in the measured range and consequently, although it makes quantitative data analysis difficult, we can be sure that it is not responsible for any of the observed maxima in the scattering. The scattering from the sample $(Bi_2O_3)_{0.68}(Er_2O_3)_{0.32}$ was intermediate in appearance between the two spectra drawn in Fig. 1.

(iii) Diffuse Scattering from $(Bi_2O_3)_{1-x}(Yb_2O_3)_x$

The elastic diffuse scattering from the bismuth–ytterbium solid solutions with $x = 0.25$ and $x = 0.35$ is plotted in Fig. 2. These data were treated in the same manner as

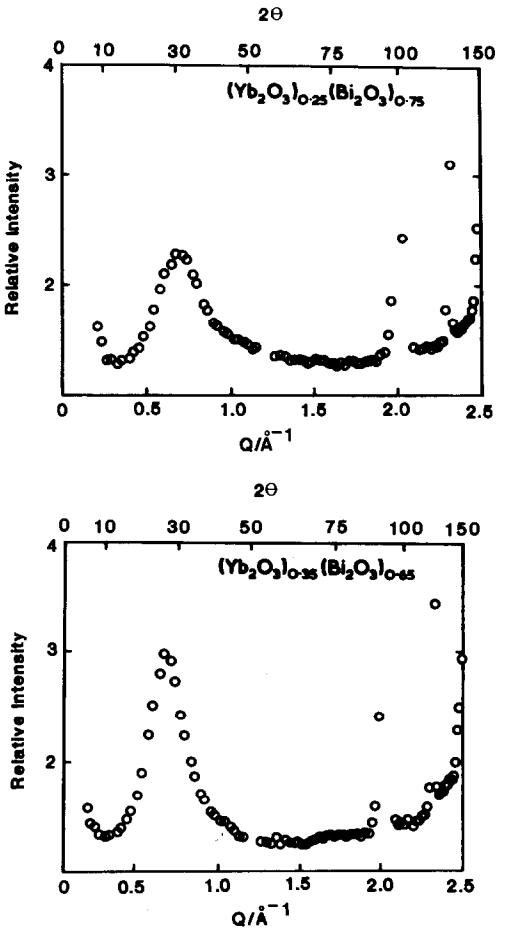

FIG. 2. Diffuse elastic scattering for $(Bi_2O_3)_{1-x}(Yb_2O_3)_x$, $x = 0.25$ and 0.35, at room temperature.

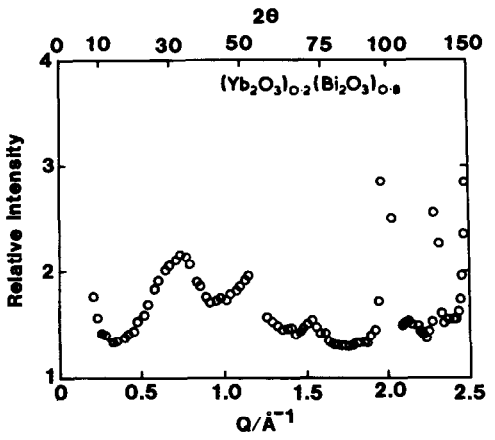

FIG. 3. Diffuse elastic scattering for $(Bi_2O_3)_{0.8}$ $(Yb_2O_3)_{0.2}$ at room temperature.

has already been described above for the Er-doped samples. As in that case, there is a strong peak at $Q \sim 0.7$ Å^{-1}. However, the maxima at $Q \sim 1.4$ and 1.7 Å^{-1} are not apparent in the scattering from the Yb^{3+}-doped materials. The sample $x = 0.30$ gave a spectrum very similar to those shown in Fig. 2. However, the sample $x = 0.20$ gave the very different spectrum that is shown in Fig. 3. A new, strong maximum is present at $Q \sim 1.15$ Å^{-1} and a weaker feature is visible at $Q \sim 1.55$ Å^{-1}.

(iv) Quasielastic Scattering from $(Bi_2O_3)_{1-x}(Er_2O_3)_x$

The data plotted in Fig. 4 represent the time-of-flight (proportional to inverse neu-

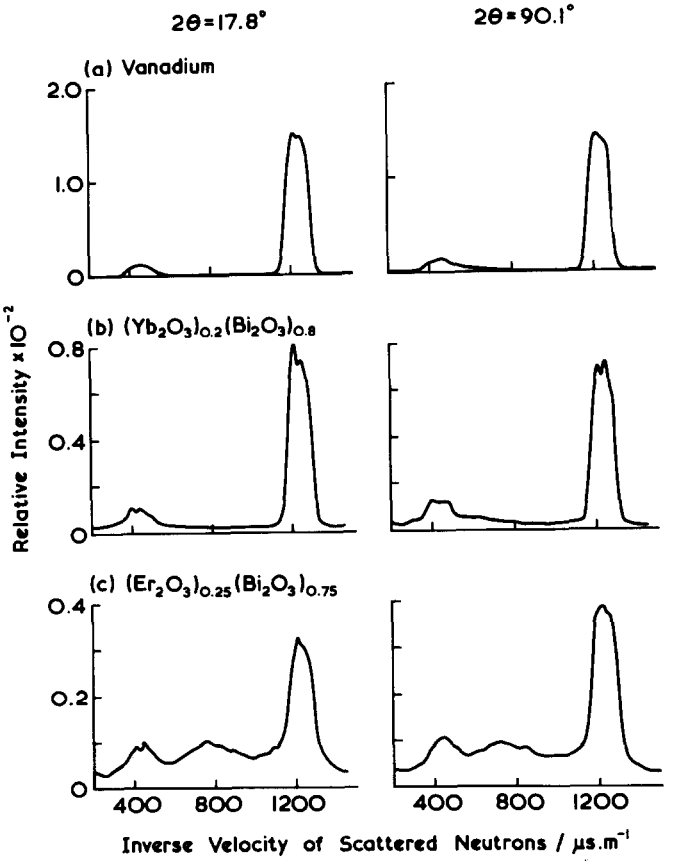

FIG. 4. Neutron count vs inverse neutron velocity (proportional to time of flight) for three different samples at each of two scattering angles.

tron velocity) taken by the scattered neutrons in reaching the detector, and the results are plotted for two different values of 2θ for each of three materials: (a) vanadium, (b) $(Bi_2O_3)_{0.8}(Yb_2O_3)_{0.2}$, and (c) $(Bi_2O_3)_{0.75}(Er_2O_3)_{0.25}$. The principal maximum in each data set corresponds to elastically scattered neutrons of wavelength 4.85 Å and the subsidiary maximum to phonon scattering. In the cases of vanadium and $(Bi/Yb)_2O_3$, these are the only clear features in the data. However, the tof spectrum of $(Bi/Er)_2O_3$ differs markedly from those of the other two samples in that there is clearly considerable scattering between the two maxima. This is quasielastic scattering and it contains information about ionic diffusion in the sample. Neutron scattering has been used to determine diffusion coefficients for many materials, e.g., for Ag^+ in the silver-ion conductor AgI (*9*), but the technique has never been applied to oxide-ion conductors. The reason for this is simply that to give rise to detectable quasielastic scattering, the diffusing ion must have a high incoherent scattering cross section; this condition is fulfilled by Ag^+ but not by O^{2-} nor by Bi^{3+}. However, Er^{3+} does have a high incoherent cross section and the results presented in Fig. 4c demonstrate unequivocally that the Er^{3+} ions play a central role in the dynamics of this material. They cannot simply be treated as a rigid framework through which the oxide ions diffuse. The motion of the Er^{3+} ions presumably represents a response to the diffusion of the anions and hence gives indirect information on the diffusion of the O^{2-} ions themselves. When these data were collected, the D7 instrument was not in the appropriate configuration to maximize tof resolution and our attempts to analyze our results quantitatively have failed, but there is clearly a possibility of studying the oxide ion transport in these materials, as a function of temperature, by using quasielastic neutron scattering techniques.

Discussion

The Bragg scattering and the diffuse scattering results on the solid solutions $(Bi_2O_3)_{1-x}(Er_2O_3)_x$ both suggest that these materials are very similar to the solid solutions $(Bi_2O_3)_{1-x}(Y_2O_3)_x$ studied previously (*3, 4*). The Bragg data on the 27% Y-doped sample showed that 2.01(6) anions per M_2O_3 formula unit occupy the regular anion site in the fluorite structure of that material, and that 0.83(6) anions per formula unit are displaced along the [111] axis to the site with coordinates (0.319(3), 0.319, 0.319); the corresponding numbers in the case of the 25% Er-doped sample are 1.97(10), 0.88(10), and (0.319(2), 0.319, 0.319), respectively. There is thus no significant difference in these parameters. Consideration of the number of displaced interstitial anions per formula unit (0.16(6) vs 0.15(10)) and the magnitude of the cation displacements along [100] 0.048(4) vs 0.045(3)) reinforces the conclusion that the average structure, as determined by neutron diffraction, is the same in these two solid solutions. The similarity between the elastic diffuse scattering results reported previously on Y^{3+}-doped Bi_2O_3 (*4*) and those presented in this paper for Er^{3+}-doped Bi_2O_3 is also striking. All the spectra contain peaks whose width is small enough to suggest that they arise from microdomains, a few unit cells in size, where there is significant local ordering. As in the case of the Y^{3+} containing samples, the three principle diffuse maxima can be indexed as the (003), (006), and $(01\bar{1})$ reflections of a rhombohedral unit cell with $a_0 \sim 4$ Å, $c_0 \sim 28.5$ Å (hexagonal setting), or as $(\frac{1}{3}\,\frac{1}{3}\,\frac{1}{3})$, $(\frac{2}{3}\,\frac{2}{3}\,\frac{2}{3})$ and (110) reflections from the cubic fluorite cell. The maxima in the scattering increase in intensity as the concentration of Er^{3+} in the solid solution increases indicative of an increase in microdomain formation. The coherent scattering lengths of bismuth and erbium are very similar to each other (and also to that

of yttrium) and it is therefore likely that the observed scattering is again produced not by ordering between Bi^{3+} and Er^{3+}, but rather by ordering between vacancies and oxide ions on the anion sublattice or by an ordering of the cation ⟨100⟩ displacements. As we have stated previously, solid solutions between Bi_2O_3 and oxides of the larger rare earths are known to have a rhombohedral unit cell very similar in size to that proposed above on the basis of the diffuse scattering results, and it is tempting to believe that small microdomains of this structure exist within the fluorite phase. The maxima in the diffuse scattering at low Q were not observed in the previous structural study on these materials (*7*).

In contrast to the results on Er^{3+}-doped Bi_2O_3, those on the Yb^{3+}-doped materials are strikingly different from those on Y^{3+}-doped Bi_2O_3. The $(003)_{rh}$ reflection is present for all samples, but for those samples with $x > 0.2$, it is the only feature visible other than the two fluorite Bragg peaks at high Q. The peak in the Yb^{3+} data is somewhat broader than that in the plots of the Er^{3+} results, suggesting that the ordered regions are smaller in size in the former case. It may well be that microdomain formation occurs on a smaller scale in the Yb^{3+}-doped material and the three-dimensional local order which is needed to define a unit cell is absent in this case. However, the presence of the $(003)_{rh}$ reflection demonstrates that some ordering takes place along the three-fold axis, which is common to both the cubic fluorite unit cell and the rhombohedral unit cell. The scattering from the sample $(Bi_2O_3)_{0.8}(Yb_2O_3)_{0.2}$ is different again. A new, sharp maximum is visible at $Q \sim 1.15$ Å^{-1} and a smaller peak is apparent at $Q \sim 1.55$ Å^{-1}. The former can be indexed as the (100) reflection from the cubic fluorite unit cell, although such a reflection is, of course, forbidden for a face-centered space group such as $Fm3m$. The origin of this peak is unclear; it may represent the nucleation of a second phase as the stability limit of the fluorite phase is reached at low dopant levels, but it is interesting that no such feature was seen in the scattering from $(Bi_2O_3)_{0.73}(Y_2O_3)_{0.27}$, on Y^{3+} composition which is only 2% above the maximum level required to stabilize the fluorite phase in the $(Bi/Y)_2O_3$ system. These observations can be explained if we recall that the coherent scattering length of ytterbium is considerably different from that of bismuth, and that neutron experiments on $(Bi/Yb)_2O_3$ are sensitive to cation ordering, unlike those on Y^{3+}- and Er^{3+}-doped materials. We propose that at low concentrations of Yb^{3+}, the Bi^{3+} and Yb^{3+} cations order in such a way as to lower the symmetry of the face-centered unit cell. For $x < 0.25$ this could be achieved, for example, by ensuring that each Yb^{3+} ion had 12 Bi^{3+} ions as nearest-neighbor cations. In simple terms, this involves putting all the Yb^{3+} ions at unit-cell corners and allowing only Bi^{3+} ions to occupy the sites at the centers of the unit cell faces (see Fig. 5). This arrangement would lead to the observation of a (100) reflection, and the feature at $Q \sim 1.55$ Å^{-1} can be indexed as the (110) reflection. The observation that this latter peak only occurs in the 20% Yb-doped sample, along with the (100) peak, leads us to conclude that in this material, unlike the Y^{3+}- and Er^{3+}-doped samples, it is a measure of

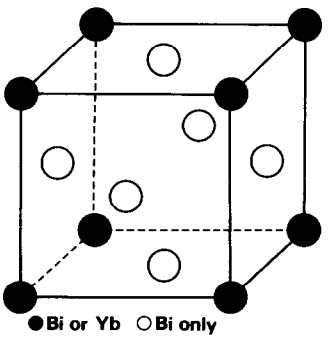

FIG. 5. A possible ordering scheme for the cation sites on $(Bi_2O_3)_{0.8}(Yb_2O_3)_{0.2}$.

cation ordering, rather than of anion ordering. It is, of course, quite possible that this type of cation ordering occurs in the Y^{3+}- and Er^{3+}-doped materials, but that it goes undetected in neutron scattering experiments for the reasons discussed above.

It is hardly surprising that Y^{3+} and Er^{3+} dopants modify the structure of δ-Bi_2O_3 in such similar ways. They both adopt the *C*-type structure in their own oxide and they have very similar ionic radii (*10*). The structural similarity would lead us to predict that $(Bi_2O_3)_{1-x}(Er_2O_3)_x$ and $(Bi_2O_3)_{1-x}(Y_2O_3)_x$ have similar ionic conductivities and, to some extent, the published data support this view. For Y^{3+}-doped materials having $x = 0.25$, the conductivity has been measured as $\sim 0.5\ \Omega^{-1}\ cm^{-1}$ at 1073 K (*11*). A very similar value has been found (*5*) for Er^{3+}-doped Bi_2O_3, again with $x = 0.25$, but an independent measurement (*12*) on the same composition has given a result of $\sim 3\ \Omega^{-1}\ cm^{-1}$. It appears that differences in sample preparation can produce nearly an order of magnitude change in the conductivity of one composition of the solid solution and we therefore feel justified in saying that Y^{3+}- and Er^{3+}-doped Bi_2O_3 have the same conductivity, within experimental error. This is to be expected in view of the structural similarities between the solid solutions. Any small difference that is present in the conductivity can be ascribed to the differences in ionic size, as reflected in the solid solution unit cell parameters, between Er^{3+} and Y^{3+}. This size difference will modify the elastic energy, and hence the activation energy, of the solid solutions (*13*).

The reduction in the extent of microdomain formation in Yb^{3+}-doped Bi_2O_3 is easily explained. The rhombohedral phase, to which we believe the microdomains are related, is formed in solid solutions between Bi_2O_3 and the oxides of the larger rare-earths. As the size of the dopant cations is reduced, the rhombohedral phase gives way to the fluorite phase, but there are still microdomains of the former phase present. As the dopant size decreases further, on going from Er^{3+} to Yb^{3+}, the stability of these microdomains decreases and they lose their three-dimensional structure until ordering is only present along the three-fold axis. It is not clear whether the cation ordering present in the 20% Yb^{3+}-doped sample is also present in the Er^{3+} and Y^{3+} solid solutions because our experimental technique is insensitive to the effect in those materials. The conductivity of $(Bi_2O_3)_{1-x}(Yb_2O_3)_x$ has been reported (*5*) as similar to that of the Er^{3+}-doped compound; hence the differences in microdomain structure do not appear to have a great effect on the conductivity. This is perhaps surprising because in both Y^{3+}- and Er^{3+}-doped Bi_2O_3, the conductivity falls as the short-range order increases with increasing dopant concentration and, furthermore, the short-range order decreases as the temperature (and hence conductivity) increase (*4*). We might thus have expected the Yb^{3+} solid solution to have a higher conductivity than those containing the other dopants. We have already noted that our Yb^{3+} samples retain the fluorite structure over a wider composition range than those made previously (*5*) and we shall therefore measure the conductivity of our samples to establish whether they behave differently to those measured in the past. It is interesting to note that the composition range reported here for the fluorite structure in Yb^{3+}-doped Bi_2O_3 is consistent with the data on other dopants reported by Iwahara *et al.* (*5*); their data on Yb^{3+} solid solutions were, by their own admission, anomalous.

Acknowledgments

We are grateful to the ILL for the provision of neutron facilities, and to Dr. A. W. Hewat and Professor O. Schaerpf for experimental assistance. During the course of this work LMM was supported by the SERC on Grant GR/C/48585.

References

1. T. Takahashi and H. Iwahara, *Mat. Res. Bull.* **13,** 1447 (1978).
2. J. A. Kilner and B. C. H. Steele, *in* "Non-Stoichiometric Oxides" (O. T. Sorensen, Ed.), Chap. 3. Academic Press, New York, 1981.
3. P. D. Battle, C. R. A. Catlow, J. Drennan, and A. D. Murray, *J. Phys. C. Sol. St. Phys.* **16,** L561 (1983).
4. P. D. Battle, C. R. A. Catlow, J. W. Heap, and L. M. Moroney, Part I, *J. Solid State Chem.* **63,** 8 (1986).
5. H. Iwahara, T. Esaka, T. Sato, and T. Takahashi, *J. Solid State Chem.* **39,** 173 (1981).
6. P. Conflant, J-C Boivin, and D. Thomas, *J. Solid State Chem.* **35,** 192 (1980).
7. M. J. Verkerk, G. M. H. van de Velde, A. J. Burggraaf, and R. B. Helmholdt *J. Phys. Chem. Solids* **43,** 1129 (1982).
8. K. D. Rouse, M. J. Cooper, E. J. York, and A. Chakera, *Acta. Crystallogr. Sect. A* **26,** 682 (1970).
9. G. Eckold, K. Funke, J. Kalus, and R. E. Lechner, *J. Phys. Chem. Solids* **37,** 1097 (1976).
10. R. D. Shannon, *Acta. Crystallogr. Sect. A* **32,** 751 (1976).
11. T. Takahashi, H. Iwahara, and T. Arao, *J. Appl. Electrochem.* **5,** 187 (1975).
12. M. J. Verkerk, K. Keizer, and A. J. Burggraaf, *J. Appl. Electrochem.* **10,** 81 (1980).
13. J. A. Kilner, *Solid State Ionics* **8,** 201 (1983).